ISSN : 0974 - 7494 Volume 9 Issue 1

Nano Science and Nano Technology
An Indian Journal

Full Paper

NSNTAIJ, 9(1), 2015 [038-047]

Influence of morphology and Particle size of tungsten trioxide (WO_3) nanocrystals on the electrochromic performances

M.A.El-Sherbiny, K.Abdullah, S.A.El-Khodary*

***Housing and Building National Research Center (HBRC), Dokki 12311, Giza, (EGYPT)**

Department of physics, Faculty of science, Al-Azhar University, Nasr city 11884 Cairo, (EGYPT)

E-mail: sherbinypsi@yahoo.com

ABSTRACT

We report herein a novel synthesis of tungsten trioxide (WO_3) nanoplate and nanosheet by thermal decomposition of tungestic acid prepared by acidic precipitation. High-resolution transmission electron microscopy (HRTEM) was used to study the crystal structure and morphology of the prepared WO_3 nanocrystals. The structure characterization and phase decomposition temperature were investigated by X-Ray diffraction (XRD), Fourier transform infrared spectroscopy (FT-IR) and differential scanning calorimetry (DSC). The WO_3 film with nanosheets structure showed a significant improved electrochromic performance with a fast coloration process and slow bleaching process with fast response time for both nanoplates and nanosheets structures.

KEYWORDS

Tungsten trioxide (WO_3);
Nanoplates;
Nanosheets;
Single crystals;
Electrochromic property.

INTRODUCTION

Shape-controlled synthesis of nanocrystalline materials is highly signiûcant, not only in terms of fundamental science but also in terms of technical applications[1]. Zero-dimensional (0D) quantum dots, synthesized by various wet-chemical routes[2], have potential applications in biological imaging and diagnostics, as magnetic nanoprobes, information storage, chemical sensors, and as highly active catalysts[3]. 1D nanocrystals (nanowires, nanorods, nanoneedles, etc.), synthesized by the vapor-liquid-solid method, the template route, or the surfactant-assisted wet-chemical route[4], have important applications in lasers, display devices, and nanoscale electriccircuits[5]. Another key category is 2D nanocrystals (nanosheets, nanodisks, and nanoplates), the speciûc crystal planes of which are highly exposed to various environments and can be utilized as active sites for catalysts and sensors[6], as well as in 2D nanodevices for electronic, magnetic, and optical applications[7]. Some 2D nanocrystals can also be used as building blocks to construct complex nanostructures[8]. Number of reports on 2D nanocrystals is limited compared with those on 0D and 1D nanocrystals[2], this may be due that, the successful synthesis of 2D nanocrystals depends on the intrinsic characteristics of the target compounds, and requires more fastidious control of the growth parameters[6].

Tungsten trioxide (WO_3) is one of the best inorganic electrochromic materials due to its high coloration efûciency and relatively low price. The electrochromic materials can be switched from transparent to coloured state by using an external voltage and a proton source. In this way, the change of state

can be described by a simultaneous injection and extraction of the electrons and protons[9,10]. This phenomenon is applied in electrochromic, photochromic and thermochromic devices, such as energy saving windows (smart windows), solar rooûng, and antiglare rear-view mirrors and gases sensors[11].

For the development of functional electronic and optical devices, WO_3 is an ideal choice. Its band gap can be tuned in the range of 2.5-3.7 eV by structural manipulations and doping[12], and can be formed into nanostructued thin films via variety methods such as thermal and electron beam evaporation[10], RF sputtering, chemical vapour deposition (CVD), anodic oxidation, sol–gel[13], spray pyrolysis[14] and magnetron sputtering[15].

In this work, WO_3 nanoplates and nanosheets were prepared by thermal decomposition of H_2WO_4. Acidic precipitation from alkali tungstate solutions were used to prepare H_2WO_4. Electrochromic characteristics of thin films prepared from these sources were investigated.

EXPERIMENTAL PROCEDURES

Preparation of WO_3 nanocrystals

The preparation of tungsten (VI) oxide nanomaterials (WO_3) involve three key steps, (i) preparation of tungstic acid (H_2WO_4) by precipitation method according to equation (1), (ii) transformations of (H_2WO_4) into $WO_3.H_2O$ nanocrystals by topochemical synthesis method with different shapes, (iii) thermal treatment to transformation of $WO_3.H_2O$ into monoclinic phase of WO_3 single-crystals.

1 Yellow tungstic acid (H_2WO_4) precipitation was obtained according to Zocher's method[17,18]. Six grams of $Na_2WO_4.2H_2O$ (BDH, England) was dissolved in 100 ml of distilled water and the solution was cooled to 5 °C. Also 25 ml of concentrated HCl cooled to the same temperature and then was added in several doses to the sodium tungestate solution. The mixture was stirred for 1.5 hour in an ice bath then for one hour at room temperature (25 °C). After decantation, the precipitate was washed three times with distilled water, then centrifuged at 2000 rpm for 20 min, and finally dried at room temperature.

2 The obtained tungstic acid (H_2WO_4) powder was dispersed in a HNO_3 aqueous solution (100 ml from 55%), stirred for 8 hours at room temperature to obtain a $WO_3.H_2O$ nanoplates (AW1) for the first sample. The second sample also dispersed in a HNO_3 aqueous solution (80 ml from 55%) and mixed with 20 ml methanol to complete the total volume 100 ml and then stirred for 8 hours at room temperature to obtain $WO_3.H_2O$ nanosheets (AW2) and then the product was washed several times by distilled water.

3 The obtained $WO_3.H_2O$ samples were sintered at 500 °C for six hours in an electric furnace and then left to be cooled down to room temperature, to get the monoclinic phase of tungsten (VI) oxide nanomaterials

$$Na_2WO_4 + 2HCl \rightarrow H_2WO_4 \downarrow + 2NaCl \quad (1)$$

Preparation of WO_3 thin films

The films of WO_3, prepared from WO_3 nanoplates (AW4) and WO_3 nanosheets (AW5) as a powder source in the present study are thermally deposited onto pre-cleaned ITO with dimensions of 1 x 2 x 0.3 cm by using a high vacuum coating unit (model E306 A, Edwards co. England); the pressure inside the chamber was pumped down to about 10^{-5} Pa before starting the evaporation process. The film thickness and rate of deposition were controlled and monitored during deposition by film thickness monitor (FTM4, Edwards co. England), where the WO_3 films thickness are about ~ 200 nm.

WO_3 nanocrystals characterizations

The crystal structures of the prepared $WO_3.H_2O$ samples were characterized using X-ray diffractometer (Philips PW3050/60) with a Cu-Ká X-ray source. Infrared absorption spectra were taken by JASCO spectrophotometer model FT/IR-6100 type A. The phase decomposition and the weight loss of $WO_3.H_2O$ were collected by Shimadzu DSC 50 thermal analyzer and Shimadzu TGA-50 whereas the microstructures were examined with a high-resolution transmission electron microscope (HRTEM, FEI Philips Tecnai G2 S-Twin operated at 200 keV). The electrochromic properties of WO_3 films were carried out by using Gamry

Full Paper

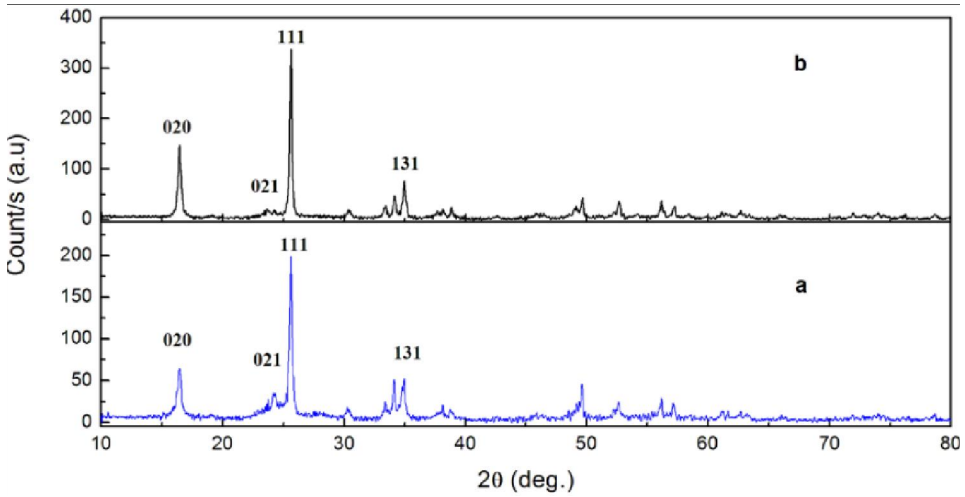

Figure 1 : XRD patterns of pure nano-structured $WO_3.H_2O$ nanoplates (a) and nanosheets (b) as prepared in powder forms

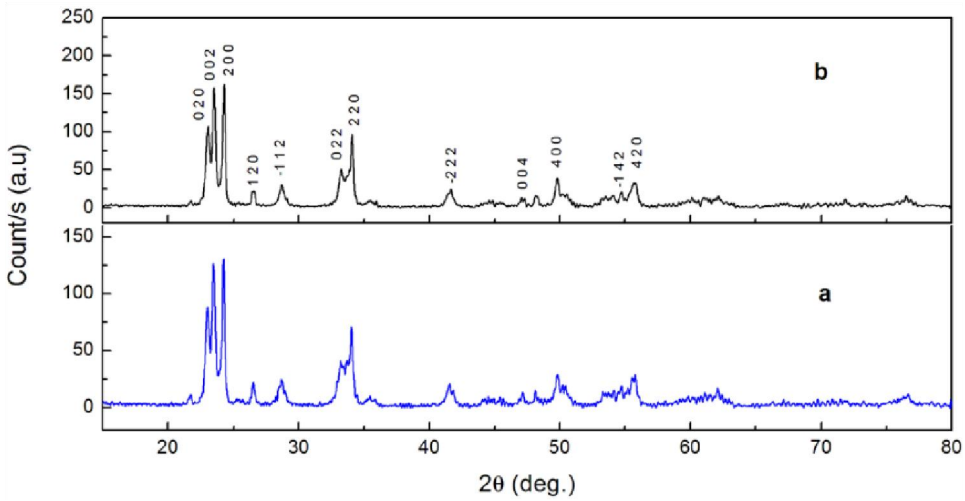

Figure 2 : XRD patterns of pure nano-structured m-WO_3 nanoplatelets (a) and nanosheets (b), after annealing at 500°C for 6 hrs in powder forms

Potentiostat / Galvanostat / ZRAG750 where ITO-back WO_3 thin film is the working electrode, 0.1M HCl is an electrolyte and serves as a H^+ ion source, the Pt disc electrode was used as a counter electrode and Ag/AgCl as a reference electrode. The thickness of the thin films was measured by Stylus method (alpha-step. Tencor instruments. Germany).

RESULTS AND DISCUSSION

Crystal structure

The crystalline phase of the prepared $WO_3.H_2O$ and WO_3 were identified by X-ray powder diffraction Figures (1) and (2), respectively. Figure (1) shows the XRD patterns performed at room temperature for pure $WO_3.H_2O$ (platelet-type sample) and (sheet-type sample) in powder form. XRD patterns of the products were exclusively orthorhombic $WO_3.H_2O$ (space group: Pnmb, a = 5.249 Å, b = 10.71 Å, c = 5.133 Å, JCPDS-ICDD 84-0886).

Four intense lines in the Figure (1, a) for the (platelet-type sample) are 3.476, 5.358, 2.569 and 3.743 Å and in Figure (1, b) for the (sheet-type sample) are 3.476, 5.378, 2.565 and 3.749 Å. These values are consistent with the standard values of 3.47, 5.36, 2.56 and 3.74 Å in JCPDS-ICDD 84-0886, corresponding to (111), (020), (131) and (021) planes. The results suggest that the platelet-type and the sheet-type nanocrystals exhibit the same crystalline phase. The intensity ratio of the peak (021) to peak (111) for the platelet-type samples is larger than that of sheet-type samples and the intensity ratio

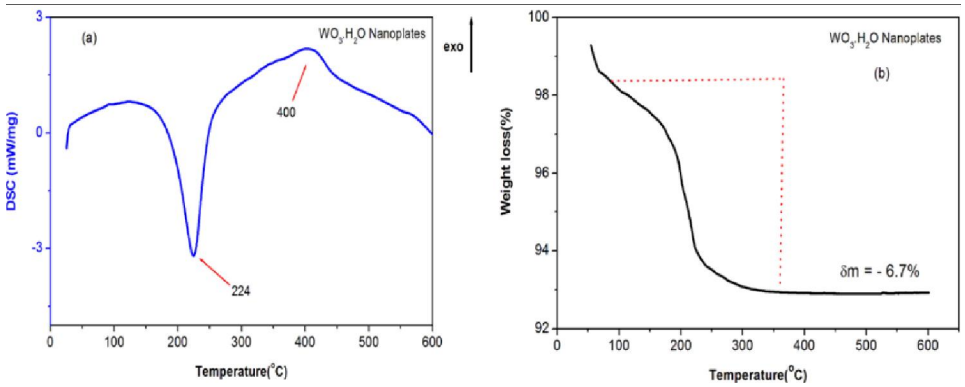

Figure 3: a) DSC and b) TGA curve of the uncalcined $WO_3.H_2O$ nanoplates respectively

of the peak (020) to peak (111) for the sheet-type samples is lager than that of platelet-type samples. This suggests that the preferred oriented planes in platelet-type $WO_3.H_2O$ are (021) planes and the abundant planes in sheet-type $WO_3.H_2O$ are (020) planes.

Figure (2) shows the XRD patterns for pure tungsten trioxide in powder forms, sintered at 500°C for six hours. As Figure (2, a) shows the XRD patterns of the WO_3 (platelet-type sample) after annealed $WO_3.H_2O$ nanoplates at 500°C for six hours; there are intense peaks at $2\theta = 23.11^o$, 23.58^o and 24.34^o, and these diffraction peaks can readily be indexed to (0 0 2), (0 2 0) and (2 0 0) reflections of monoclinic WO_3 phase. No peaks associated with other compounds were detected, indicating that the WO_3 product is a pure phase. The diffraction lines are completely matched with XRD card number (space group: P21/n, a = 7.306 Å, b = 7.540 Å, c = 7.692 Å, JCPDF – ICDD 72-0677). According to its XRD results, the cell parameters of the WO_3 nanoplates are calculated to be a = 0.7306 nm, b = 0.7545 nm, C = 0.7701 nm, and â = 90.809 (°), which are close to the literature values (a = 0.7306 nm, b = 0.7540 nm, C = 0.7692 nm, and â = 90.881 (°))

Figure (2, b) also shows the monoclinic phase of WO_3 (sheet-type sample) after annealed $WO_3.H_2O$ nanosheets at 500°C for six hours, and also have the same matched XRD card (space group: P21/n, a = 7.306 Å, b = 7.540 Å, c = 7.692 Å, JCPDF – ICDD 72-0677) corresponding to the intense peaks at 2è = 23.11°, 23.58° and 24.34°. No H_2WO_4 peaks are observed, implying the precursors have been completely converted into m-WO_3 via heat treatment. In addition, the cell parameters of the WO_3 nanosheets are calculated to be a = 0.7298 nm, b = 0.7560 nm, C = 0.7696 nm, and â = 90.709 (°).

Thermal analysis

In order to determine the appropriate temperature for thermal conversion of the precursor $WO_3 \cdot H_2O$ into WO_3, the thermal behavior of the precursor was investigated. The thermo gravimetric analysis (TGA) and differential scanning calorimetric (DSC) curves of

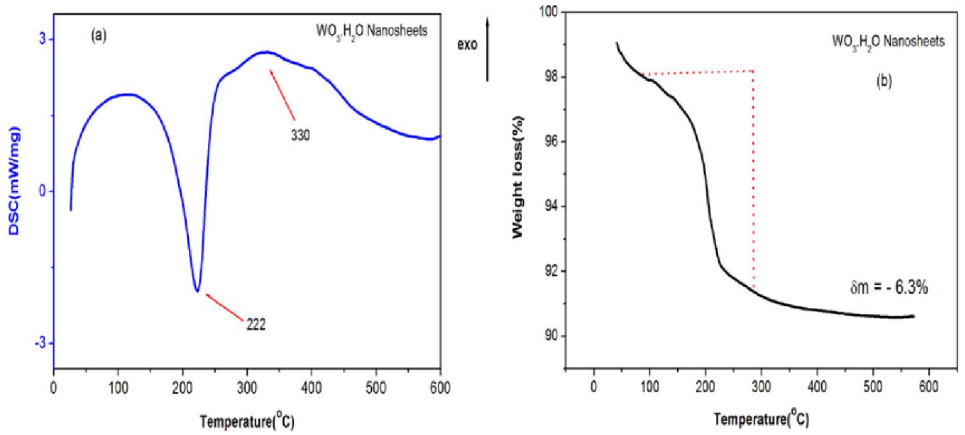

Figure 4: a) DSC and b) TGA curve of the uncalcined $WO_3.H_2O$ nanosheets respectively

Full Paper

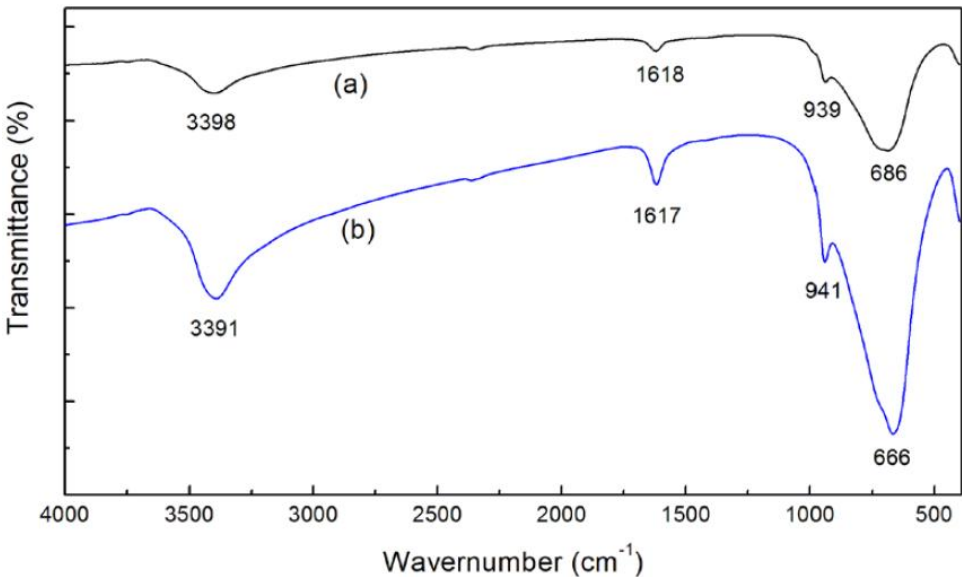

Figure 5: FT-IR spectra of $WO_3.H_2O$ nanoplates (a) and $WO_3.H_2O$ nanosheets (b)

the precursor are shown in Figures (3, b & 4, b) and (3, a & 4, a), respectively. Mass losses of ~ 6.7% and~ 6.3% for nanoplates and nanosheets, respectively, as shown from Figures (3, b & 4, b) are associated to the dehydration precursor and which are in agreement with the theoretical calculation (7.2%) for the $WO_3 \cdot H_2O$ structure[19].

The temperature of onset water loss was found to be morphological dependent. It was observed between 195-211 °C for nanoplates and 188-200 °C for nanosheets and occurs in several steps corresponding water loss of physically adsorbed water and tungsten acid decomposition.

The large and sharp endothermic peak at 224°C in Figure (3, a) and 222°C in Figure (4, a) can be ascribed to the $WO_3 \cdot H_2O$ decomposion and the loosely bound coordinated water. The relatively small exothermic peak at about 400°C for $WO_3 \cdot H_2O$ nanoplates and 330°C for $WO_3 \cdot H_2O$ nanosheets probably comes from the phase transformation of the samples from orthorhombic $WO_3 \cdot H_2O$ to monoclinic WO_3. Based on TGA/DSC results, samples were treated at 500°C for 6 hrs-to ensure the fully transformation to m-WO_3.

Fourier transforms infrared (FT-IR) analysis

The infrared technique has been used to confirm the molecular structure of tungsten oxide hydrates $WO_3.H_2O$ and tungsten trioxide (WO_3). Figure (5) shows the FT-IR spectra of as-deposit pure $WO_3.H_2O$ nanoplates and nanosheets. Large broad intensity peak around 3398 cm^{-1} for $WO_3.H_2O$ nanopaltes and 3391 cm^{-1} for $WO_3.H_2O$ nanosheets have been observed and assigned as ν (OH) stretching modes of surface adsorbed water molecules. The bands located at 1618 cm^{-1} for $WO_3.H_2O$ nanoplates and 1617 cm^{-1} for $WO_3.H_2O$ nanosheets are assigned as $\delta(H_2O)$ bending modes of water molecules. These results are in accordance with Daniel's[20] IR data reported on tungsten oxide hydrates. These peaks must be disappeared in WO_3 IR spectra but this occurred.

We observed that a small-intensity peak at 3439 cm^{-1} for WO_3 nanoplates and also at 3438 cm^{-1} for WO_3 nanosheets, these are assigned as (OH) stretching modes of surface adsorbed water molecules (moisture content), and this is due to insufficient drying of the sample before measurement (see Figure 6).

Figure (5, a) shows two sharp intense bands at 939 cm^{-1}, 686 cm^{-1} for $WO_3.H_2O$ nanoplates, the former 939 cm^{-1} can be ascribed to the symmetric stretching vibrational mode of terminal (W=O) bond. Also in Figure (5, b) we have two bands at 941 and 666 cm^{-1} for $WO_3.H_2O$ nanosheets, the band at 941 cm^{-1} is also assigned to (W=O) stretching mode[18, 20 and 21].

These peaks at (W=O) does not observed in m-WO_3 spectra as expected. Two peaks at 686 and 666 cm^{-1} arise from the stretching modes of (O-W-O) bridging oxygen[20], these bands are assigned to the O-

TABLE 1 : Assignment and vibrational band frequencies (ν) obtained from ($WO_3.H_2O$) nanomaterials and (m-WO_3) nanomaterials

Nanomaterials / Attribution	$WO_3.H_2O$ Nanoplates (cm^{-1})	$WO_3.H_2O$ Nanosheets (cm^{-1})	WO_3 Nanoplates (cm^{-1})	WO_3 Nanosheets (cm^{-1})	Reference of $WO_3.H_2O$	Reference of WO_3
ν (OH)	3398	3391	3439	3438	[18, 20,21]	--
$\delta(H_2O)$	1618	1617	--	--	[18, 20,21]	--
ν (W=O)	939	941	--	--	[18, 20,21]	[23]
ν (O-W-O)	686	666	817 754	816 753	[18, 20,21]	[20, 23] [20, 23]

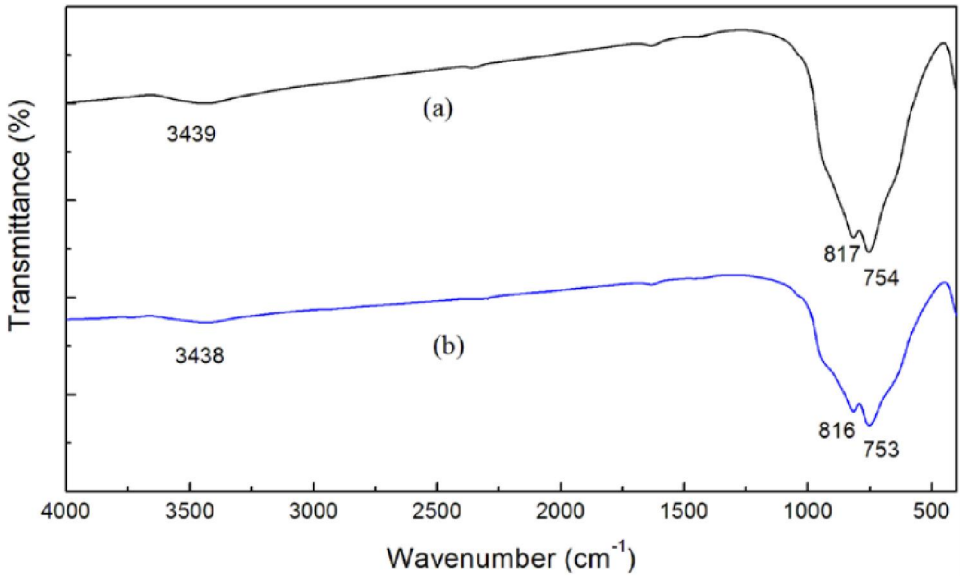

Figure 6: FT-IR spectra of WO_3 nanoplates (a) and WO_3 nanosheets (b)

W-O bridging mode of the W-O_6 corner sharing species[22] and these peaks are strongly affected by heat treatment at 500°C. Figure (6, a) and (6, b) shows the spectra have a broad band with two weak maxima at 817 and 754 cm^{-1} for m-WO_3 nanoplates and at 816 cm^{-1} and 753 cm^{-1} for m-WO_3 nanosheets corresponding to crystalline WO_3[21,23]. All the IR data for $WO_3.H_2O$ and m-WO_3 are reported in TABLE 1.

Morphology and microstructure

To investigate the overall morphologies of the samples, the obtained samples are investigated by HRTEM. Figure 7(a & b) shows TEM images of the sample synthesized by dispersion of $WO_3.H_2O$ in a HNO_3 aqueous solution. Clearly, the TEM micrographs of Figure 7(a & b) revealed that the as prepared $WO_3.H_2O$ sample has irregular square nanoplates. After calcined at 500°C Figure 7(c & d) it can be seen that the nanoparticles adhere each other and a great variety of the morphology happened from irregular square shape to ovoid shape and that is occur as a result of the calcination temperature.

Figure 8 (a-c) shows the TEM micrographs of the sample synthesized by dispersion of $WO_3.H_2O$ in a HNO_3 aqueous solution (80 ml from 55% HNO_3 and mixed with 20 ml methanol alcohol to complete the total volume 100 ml). The low magnification of TEM image shows that the $WO_3.H_2O$ in the irregular square shape transformed to the rectangular shape to be a rectangular nanosheets according to the shadow cross area of two sheets as shown in Figure (8b) and the images including some nanorods. After calcinations at 500°C, Figure 8 (d & e) show that there is no change in the morphology of the

Full Paper

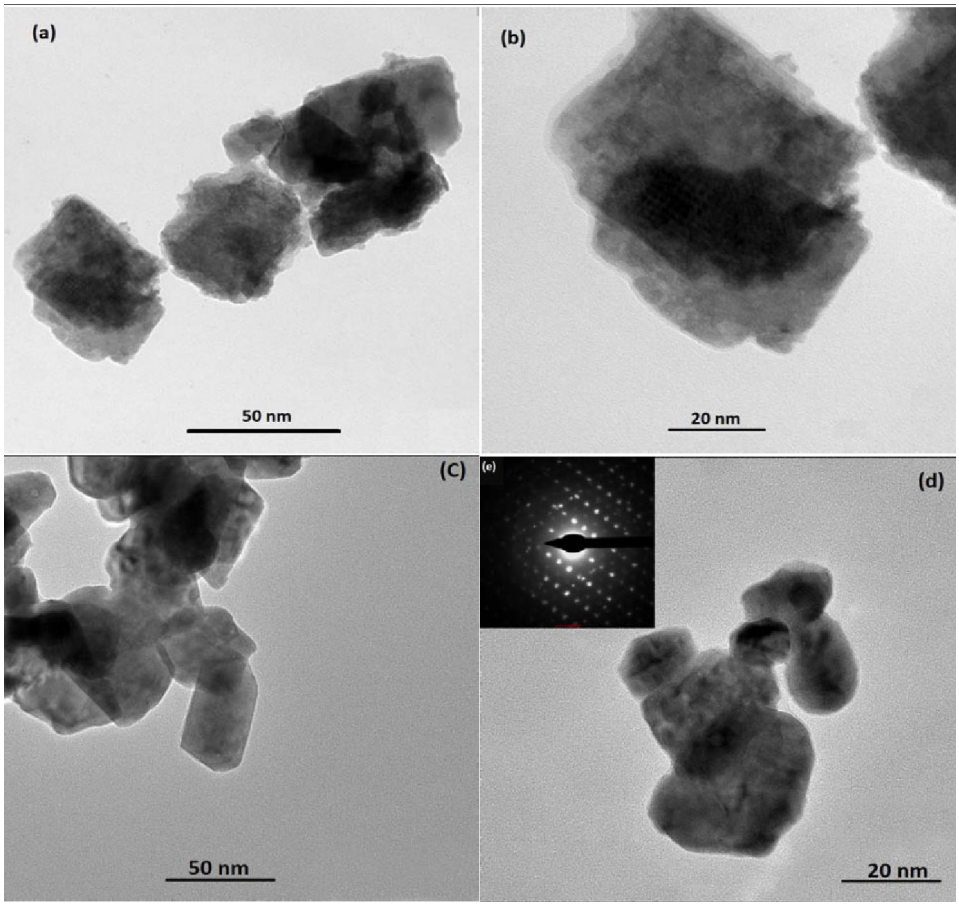

Figure 7: (a and b) TEM images of the as prepared tungstic acid $WO_3.H_2O$ nanoplates; (c and d) the WO_3 nanoplates after calcination at 500°C and (e) SAED of the sample (inset in d)

nanoparticles which still in the shape of rectangular nanosheets, whereas the nanorodes disappeared. The SAED patterns (the inset in Figure 7(d) and Figure 8 (e).) shows the uniform, wide and ordered diffraction spots can be assigned to a single-crystalline WO_3 nanoplates and nanosheets, respectively.

Electrochromism characterization

(a) Cyclic-voltammetry (CV)

Cyclic voltammetry (CV) was used to achieve the electrochemical properties of WO_3 thin films under oxidation state. The electrochromic properties of WO_3 thin films were studied by using a three electrode electrochemical cell containing 0.1M HCl from (33% HCl) electrolyte solution (buffer solution), the WO_3 films on ITO substrates were used as the working electrode, a Pt disc auxiliary electrode used as a counter electrode and Ag/AgCl as a reference electrode. The processes of ion intercalation and deintercalation was noted after activating the working electrode electrochemically prior to measurements by applying 10 cyclic scans from -0.6V to 0.6V with a sweep rate 100 mV/S as shown in Figure (9) for different WO_3 thin film systems.

The current resulting from this scan rate was measured during both the ion intercalation and deintercalation denoted as cathodic spike current density (J_{Pc}) and anodic peak current density (J_{Pa}), respectively. The diffusion coefficient (D) of H^+ ions during intercalation and deintercalation can be calculated from the Randles - Sevcik equation[24], depending on the cathodic and anodic peak current density (J_{Pc} and J_{Pa}).

$$j_p = 2.72\times10^5\ n^{3/2}\ D^{1/2}\ C_o\ \delta^{1/2} \qquad (2)$$

where D is the diffusion coefficient, n is the number of electrons transferred in unit reaction, C_o is the concentration of active ions in the solution and ð is the scan rate. The effective diffusion coefficients were calculated from equation (2) to be 1.52×10^{-15} and 8.56×10^{-17} cm^2s^{-1} for intercalation and deintercalation processes, respectively, form WO_3 thin film prepared

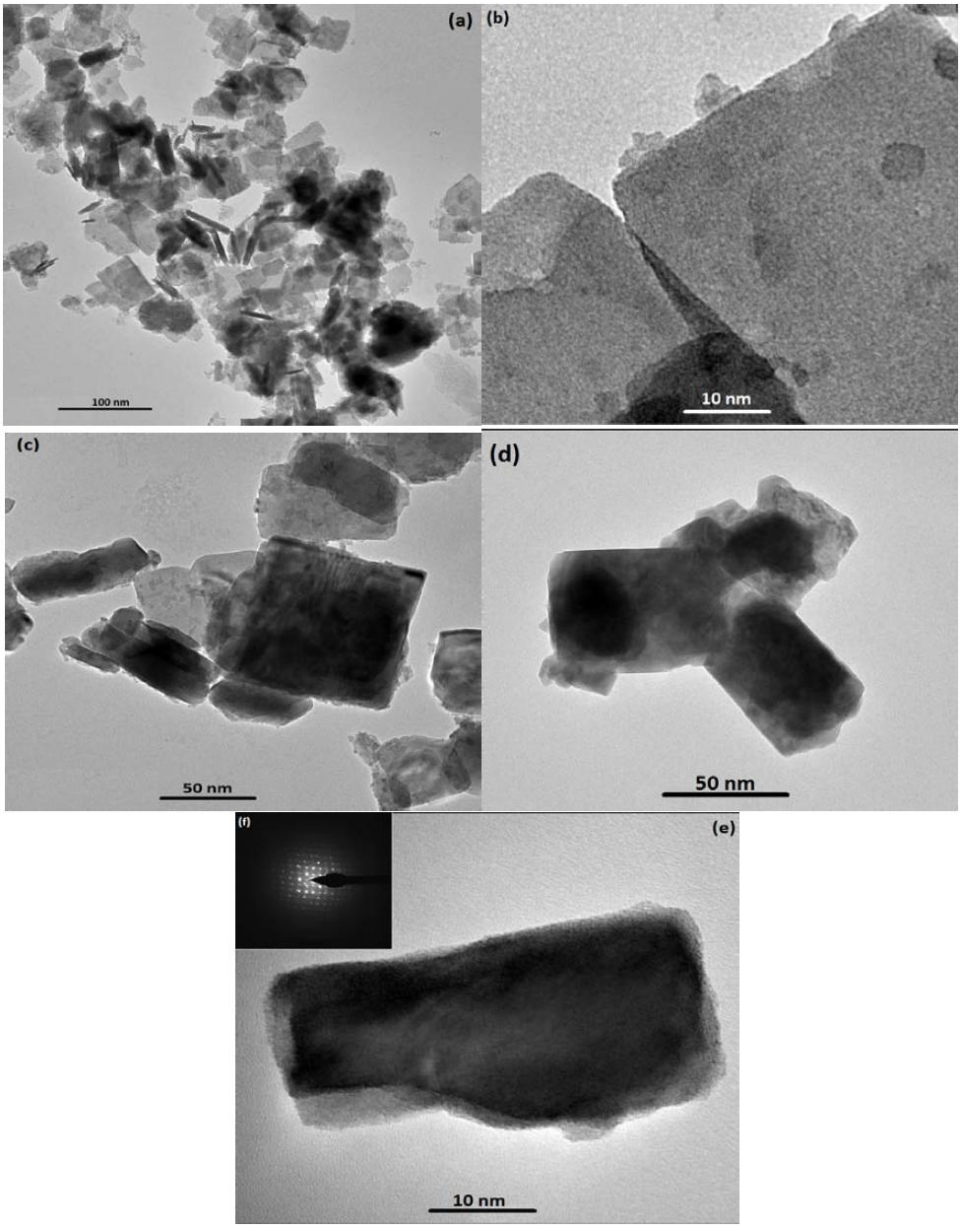

Figure 8 : (a-c) TEM images of the as prepared tungstic acid $WO_3.H_2O$ nanosheets; (d and e) the WO_3 nanosheets after calcination at 500°C and (f) SAED of the sample (inset in e)

from (platelet-type sample) AW4 as a powder source. Also, the calculated D-values are formed to be 1.30×10^{-13} and 7.69×10^{-15} cm^2s^{-1} for intercalation and deintercalation processes, respectively, for WO_3 thin film prepared from (sheet-type sample) AW5 as a powder source.

Figure (9, b) also reveals that multiplication of the current density for the WO_3 thin film leads to increase the intercalation and deintrecalation of H^+ ions into and out the film. This means the enhancement of oxidation and reduction processes (redox), which confirm their perfect electrochemical properties of the WO_3 thin film prepared from (sheet-type sample) AW5 as a powder source.

(b) Chronoamperometry (CA)

Figure (10) shows the data on switching response of the current-time dependence under application of step voltage -0.6V and +0.6V for WO_3 thin films. It was observed that the time duration was 10 seconds for all samples, but for WO_3 thin film prepared from (sheet-type sample) AW5, the current density is higher than that of nanoplates WO_3 thin film Figure (10, b). This is in agreement with the cyclic voltammetry (CV)

Full Paper

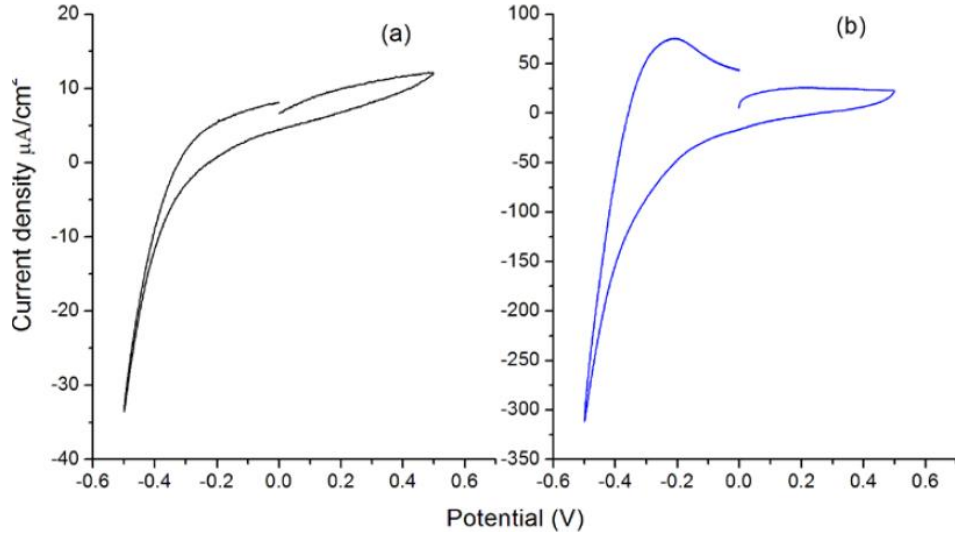

Figure 9: Cyclic voltammograms of WO_3 nanoplates (AW4) (a) and WO_3 nanosheets (AW5) (b) in 0.1M HCl from (33% HCL) with the scan rate 100 mV/s

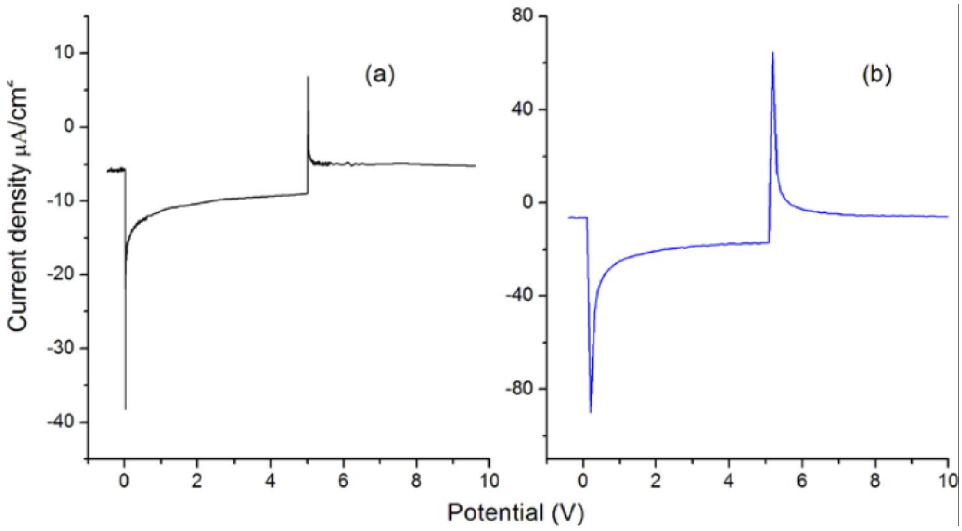

Figure 10: Chronoamperometry of WO_3 nanoplates (AW4) (a) and WO_3 nanosheets (AW5); (b) in 0.1M HCl from (33% HCL) with the scan rate 100 mV/s

results discussed before in section (4.7.1).

CONCLUSIONS

Synthesis of single-crystalline WO_3 nanocrystals through a topochemical method had been developed by conversion process of the obtained H_2WO_4 nanoplates into WO_3 nanoplates and H_2WO_4 nanosheets into WO_3 nanosheets, respectively, via calcinations at high temperature in air. This synthetic method is simple, mild, controllable, and it provides a novel method for preparations of two-dimensional nanostructures. The WO_3 thin film with nanosheets structures exhibited a unique electrochromic property because of quantum size confinement of nanosheets. Furthermore, the nanosheets film exhibited a fast coloration process and slow bleaching process and that is all controlled by a diffusion mechanism. The electrochromic ûlms based on WO_3 nanosheets with a unique electrochromic property may ûnd potential applications in special energy-saving windows and other instruments.

REFERENCES

[1] J.Jortner, C.N.R.Rao; Pure Appl.Chem., **74**, 1491 **(2002)**.

[2] X.Wang, J.Zhuang, Q.Peng, Y.Li; Nature, **437**, 121 **(2005)**.
[3] K.Watanabe, D.Menzel, N.Nilius, H.J.Freund; Chem. Rev., **106**, 4301 **(2006)**.
[4] Y.Xia, P.Yang, Y.Sun, Y.Wu, B.Mayers, B.Gates, Y.Yin, F.Kim, H.Yan; Adv.Mater., **15**, 353 **(2003)**.
[5] M.Law, D.J.Sirbuly, J.C.Johnson, J.Goldberger, R.J.Saykally, P.Yang; Science, **305**, 1269 **(2004)**.
[6] K.Izawa, T.Yamada, U.Unal, S.Ida, O.Altuntasoglu, M.Koinuma, Y.Matsumoto; J. Phys. Chem. B., **110**, 4645 **(2006)**.
[7] M.Osada, Y.Ebina, K.Fukuda, K.Ono, K.Takada, K.Yamaura, E.Takayama-Muromachi, T.Sasaki; Phys. Rev. B., **73**, 153301 **(2006)**.
[8] L.Li, R.Ma, N.Iyi, Y.Ebina, K.Takada, T.Sasaki; Chem. Commun, **29**, 3125 **(2006)**.
[9] C.M.Lampert, C.G.Granqvist (Eds); Large Area Chromogenics Materials and Devices or Transmittance Control, SPIES4, Optical Engineering Press, Bellingham, USA **(1989)**.
[10] A.Agrawal, J.P.Cronin, R.Zhung; Sol. Energy Mater, **31**, 9 **(1993)**.
[11] A.Hoel, L.B.Kish, R.Vajtai, G. A.Niklasson, C.G.Granqvist, E.Olsson; Mater. Res. Soc. Symp. Proc., **581**, 15 **(2000)**.
[12] S.K.Deb; Solar Energy Mater. & Solar Cells, **92**, 245 **(2008)**.
[13] E.Özkan, F.Z.Tepehan; Sol. Energy Mater. Sol. Cells, **68**, 265 **(2001)**.
[14] M.Regragui, M.Addou, A.Outzourhit, Elb.El-Idrissi, A.Kachouane, A.Bougrine; Sol. Energy Mater. Sol. Cells, **77**, 341 **(2003)**.
[15] A.A.Akl, H.Kamal, K.Abdel-Hady; Physica B., **325**, 65 **(2003)**.
[16] H.Zocher, K.Jacobson; Kolloidchem. Beih., **28(6)**, 167 **(1929)**.
[17] Cs.Balázsi; Materials Structure, **6(2)**, 135 **(1999)**.
[18] Xiaolan Wie, Peikany Shen; Electrochemistry communications, **8**, 293 **(2006)**.
[19] M.F.Daniel, B.Desbat, J.C.Lassegues, B.Gerand, M.Figlarz; J. Solid State Chem., **67**, 235 **(1987)**.
[20] A.Cremonesi, D.Bersani, P.P.Lottici, Y.Djaoued, P.V.Ashrit; J. Non. Cryst. Sol., **345&346**, 500 **(2004)**.
[21] M.Deepa, P.Singh, S.N.Sharma, S.A.Agnihotry; Sol. Engy. Mater. Sol. Cells, **90**, 2665 **(2006)**.
[22] Bridget Ingham, Shen V.Chong, Jeff L.Tallon; J. Phys. Chem. B, **109**, 4936 **(2005)**.
[23] G.Granqvist; Hand book of Inorganic Electrochromic Materials, Elsevier, Amsterdam **(1995)**.